EFDA–JET–PR(06)20

Yu.F.Baranov and JET-EFDA Contributors

On Electron Heat Pulse Propagation in JET H-Mode and Optimised Shear Discharges

On Electron Heat Pulse Propagation in JET H-Mode and Optimised Shear Discharges

Yu.F.Baranov and JET-EFDA Contributors*

EURATOM/UKAEA Fusion Association, Culham Science Centre, Abingdon, Oxon, OX14 3DB, UK
** See annex of J. Paméla et al, "Overview of JET Results ", (Proc. 20th IAEA Fusion Energy Conference, Vilamoura, Portugal (2004)).*

Preprint of Paper to be submitted for publication in
Plasma Physics and Controlled Fusion

ABSTRACT.
Electron heat pulse propagation in JET H-mode and ITB plasmas was analysed using the TRANSP code and ECE measured electron temperature. The heat pulse caused by ELMs in standard H-mode and hybrid scenario discharges propagate in accordance with the Critical Gradient Model (CGM). The electron temperature profile stiffness is typically observed in the plasma above criticality in the outer half of the plasma radius and disappears in the core. The analysis allows determination of the critical value of R/L_{Te} and the stiffness factor. The theoretical predictions based on the trapped electron mode model were compared with the experimentally deduced parameter R/L_{Te}. Electron temperature profile stiffness factor was found to be of the order of one in the outer half of the plasma radius and decreasing in the core. The same technique has been applied to ITB plasmas. The critical gradient model is inapplicable for description of electron heat flux variations inside ITB caused by large type-I ELMs. Temperature perturbations are strongly damped inside an ITB. The CGM can be applied in the region between ITB and the plasma periphery. The stiffness factor deduced from experimental data are close to or slightly above of what is observed in standard H-mode plasma.

INTRODUCTION.
Results of investigation of heat pulse propagation have been reported in a number of papers [1-12]. Electron temperature profile stiffness has been observed and a semi-empirical model proposed for description of the heat flux [1,4,11,12]. In this paper we present results of analysis of the heat flux perturbation caused by ELMs. Heat pulse propagation is investigated in JET optimised shear and standard H-mode discharges. Electron heat transport is analysed on the basis of TRANSP modelling [14]. Heat pulse propagation is investigated during quiescent periods between ELMs or in the presence of small grassy ELMs. An analysis of the transport properties with TRANSP code is performed using ECE measurements for electron temperature at 0.5ms time and 2-4cm space resolution. Electron density is deduced from the Thomson scattering and interferometer measurements and ion temperature is obtained from the charge-exchange measurements. Fast magnetic measurements are used to define plasma boundary with time resolution better than 1ms. Plasma equilibrium is calculated by the TRANSP code every 1ms taking into account a variation of the plasma boundary and pressure. The ion temperature measured by the charge exchange diagnostic is available on a 40-50ms time grid. The heating power deposition is affected to some extent by ELMs due to density variation and redistribution of the fast particles. We analysed pulses with core power deposition, where density variation is relatively small. The TRANSP modelling does not take into account a possible redistribution of the fast particles by ELMs. However, there is no experimental evidence that such a process is significant in the plasma core. The TRANSP code adequately describes all important processes involved in the electron and ion power balance [14].

1. ELECTRON HEAT FLUX IN HYBRID SCENARIO OR STANDARD H-MODE DISCHARGE WITH SAWTEETH.

As mentioned above we were interested in the characteristics of the electron heat flux during a quiescent period between ELMs. We begin this section with analysis of the hybrid scenario discharge #62494 with a current of 2MA, a magnetic field 2.4T [15]. There are two quasi-steady state phases in this pulse. They are characterised by different levels of NBI power, which varies from 12MW in the first phase (6.5s<t<10.5s) to 19MW in the second phase (10.5s<t<14.5s). There was 5-10% decrease in the plasma density, 10-20% increase in T_e and 20-30% increase in T_i with transition from the first to the second quasi-steady phase. Electron heat flux propagation was analysed in these two phases. A variation in the electron temperature profile, electron heat flux, diffusivity and D_α signal are shown in Fig.1 for a short period of time including two ELMs. The time evolution of these parameters is very similar in both quasi-steady state phases and therefore we showed only the first one. Each ELM causes a sharp increase in the heat flux. When the D_α signal drops roughly to its background level (5ms after the ELM starts), the electron heat flux gradually decreases until next ELM strikes. Short bursts of the heat flux radially extended from the core to the periphery can be seen on the contour plot of q_e (Fig.1f). The amplitude of the bursts decreases with time between successive ELMs. The variation of the normalised heat flux $q_e / (n_e T_e^{5/2})$ as a function of local R/L_{T_e} is shown in Fig.2 by solid lines for different quasi-state phases (fig.2a and b) and for several radial locations. Short period of time $\Delta t \approx 5$ms following after each ELM corresponding to the ballistic phase [10] is excluded from our consideration. It should be noted that the plasma density variation caused by each ELM does not exceed 10% in the region of r/a<0.75, which is investigated in this paper. It follows from the reconstruction of the density profiles by Abel inversion of the line integrated density, obtained by interferometer measurements. The uncertainty in the density leads to an error in the flux calculation of the order of 10% which is significantly smaller than the range of the flux variation shown in Fig.1 and 2. Heat flux variation with R/L_{T_e} described by the critical gradient model [11-17] was compared with a variation of the heat flux deduced from the experiment. . In the framework of the theory the electron heat flux can be expressed in the following way [18]:

(1)

where q is the safety factor, $\rho_s = (m_i T_e)^{1/2} / eB$, C the stiffness factor, χ_0 the residual diffusivity and H is a Heaviside function. Formula (1) was used to find the best fit (corresponding to $\min(\chi^2)$) for the experimental dependence of $q_e / (n_e T_e^{5/2})$ on R/L_{T_e} assuming that the residual flux $\chi_0 \delta T_e / \delta r$ is much smaller than q_e. The dashed and dotted lines in Fig.2 show the approximations found in this way. Parameters C and $(R/L_{T_e})_{cr}^{exp}$ were deduced from the best fit. They are presented with the standard deviations in parenthesis in the Table 1 and Table 2 for the time intervals 8.827s<t<8.860s and 11.515s<t<11.540s, respectively, and fig.3. The standard deviation and $\min(\chi^2)$ are shown for $F = (q_e / (n_e T_e^{5/2})) / \max(q_e / (n_e T_e^{5/2}))$. It should be noted that the heat flux dependence on the R/L_{T_e} becomes irregular in the plasma core (r/a)<0.3-0.4, especially during the second time interval 11.515s <t< 11.540s. Large noise type fluctuations on the heat flux signal, probably, can be attributed

to the bursts of fishbone MHD, which are localised in the region between magnetic axis and R=3.45m. The standard deviations in these region are very large as can be seen for R=3.36,3.46m in Table 2. These fluctuations make definition of C and $(R/L_{T_e})^{exp}_{cr}$ inaccurate and they are not shown in Fig.3. Outside the plasma core the stiffness factor C is of the order of one. The 'experimental' $(R/L_{T_e})^{exp}_{cr}$ ratio does not change significantly with a transition from the first time interval to the second one for all radial points but one.

Two different predictions for the critical value of R/L_{T_e} based on TEM mode theory [7] and [13] were used by authors in [11] and [18]. According to [7] and [13] the critical value can be expressed, respectively, in the following way (There is a misprint in eq.(2c) of ref.13. The correct expression is given by eq.(5) of ref.[11].):

$$(R/L_{T_e})^{th}_{cr1}=(0.357\sqrt{\varepsilon}+0.271)(4.9-1.31R/L_n+2.68s+\ln(1+20\nu_{eff}))/\sqrt{\varepsilon}, \quad (2)$$

$$(R/L_{T_e})^{th}_{cr2}=2L_B/3L_n+20(1-f_t)/9f_t+f_t/2(1-f_t)(1-L_B/2L_n)^2, \quad (3)$$

where $L_n = (n_e/(\delta n_e/\delta r))$, $L_B = R$, $\varepsilon = r/R$, $\nu_{eff} \approx 0.1Rn_eZ_{eff}/T_e^2$ and f_t is a fraction of trapped electrons. The derivatives are calculated using minor radius defined as $r = (R_{out}-R_{in})/2$, where R_{out} and R_{in} are the radii of the flux surface on the low and high field side. Expressions (2) and (3) are not applicable in the case low magnetic shear s<0.5. The theoretical predictions and corresponding parameters deduced from the experimental data are compared in Table 1 and 2. The error bars reflect the variation of the parameters between ELMs in formulas (2) and (3). The comparison of $(R/L_{T_e})^{exp}_{cr}$ with $(R/L_{T_e})^{th}_{cr}$ indicates that there is a discrepancy between the theoretical and experimental values. It should be noted that expression (2) defines so called 'apparent' critical value of $(R/L_{T_e})^{th}_{cr1}$, which is 10-20% larger than the real threshold value [7]. This factor moves the $(R/L_{T_e})^{th}_{cr1}$ estimate closer to $(R/L_{T_e})^{exp}_{cr}$. Density gradient produces a stabilising effect in eq.(3). It is responsible for an anomalous increase in $(R/L_{T_e})^{th}_{cr2}$. It reflects a limitation of applicability of the model [13] for $R/L_n>1$.

Qualitatively, very similar behaviour was observed in standard H-mode discharge with sawteeth at a magnetic field of $B_o = 2.3$T, plasma current of $I_p = 1.4$MA and neutral beam heating power of $P_{NB} = 14$MW. Fig.4 shows a variation of the T_e profile and of the heat flux q_e between two successive type-I ELMs in Pulse No: 61520. A variation of the normalised heat flux $q_e / (n_eT_e^{5/2})$ as a function of R/L_{T_e} is shown in Fig.5 by solid lines for several radial locations. Dashed lines show best fit of approximation (1) for the normalised flux. The parameters $(R/L_{T_e})^{exp}_{cr}$, C deduced from the best fit and theoretical predictions [7,13] for $(R/L_{T_e})^{th}_{cr1,2}$ are shown in Table 3. In the region of R = 3.46-3.66m the electron temperature profile is stiff and can be described in the framework of the critical gradient model, which is corroborated by reasonable agreement between q^{exp}_e and q^{th}_e as defined by formula (1). The stiffness factor is of the order of 1 in the outer half of the minor plasma radius and decreases to the plasma core. Applied procedure gives a negative value of $(R/L_{T_e})^{exp}_{cr}$ and a large standard deviation at R = 3.36m, which indicates that the plasma is below criticality in this region. Fig.6 shows comparison

of the stiffness parameters deduced from the experiment and from theory in the region above criticality. There is in general disagreement between theory prediction [7,13] for the critical $(R/L_{T_e})^{th}_{cr1,\,2}$ and experimental $(R/L_{T_e})^{exp}_{cr}$.

The magnitude of the stiffness factor for the outer half of the minor plasma radius deduced in our analysis is in agreement with data reported in [9].

2. ELECTRON HEAT FLUX IN DISCHARGE WITH ITB.

To analyse electron temperature profile stiffness in ITB plasmas we have applied the same technique as in the case of standard H-mode discharges. Namely, the heat pulse propagation between temperature perturbation caused by ELMs or internal reconnections was modelled. Typically, strong ITBs can coexist with relatively small type-III ELMs. Larger type-I ELMs often significantly erode or even destroy ITBs [10]. The variation of the plasma transport properties in the presence of type-I ELMs was analysed for the case of strong ITBs, which were formed in reversed shear Pulse No: 51573. The existence of ITBs was identified using a ρ^* criterion [19]. The analysed discharge was performed at $B_o = 2.6T$, $I_p = 2.2MA$, $P_{NB} = 12MW$, $P_{ICRH} = 5MW$ and $P_{LH} = 2MW$. Electron temperature evolution is shown in Fig.7a,c for a time interval, which begins with small type-III ELMs ($t<6.45s$) and ends with large type-I ELMs after $t>6.45s$ (see Fig.7b). Temperature perturbations caused by small ELMs can be seen only in the plasma periphery for $R>3.6m$. The large temperature gradient in the region of outer ITB around $R = 3.56m$ experiences relatively small variation before the start of the first large ELM at $t = 6.48s$, as can be seen from Fig.7c. Large ELMs significantly perturb the temperature. Perturbations penetrate deep into the plasma. The steepness of the T_e profile is reduced after the first large ELM (compare profiles at $t = 6.44s$ and $6.50s$ in Fig.7c). The ITB, however, survived although its strength (T_e profile steepness) was reduced. The second type-I ELM at 6.66s reduced even further the T_e gradient to such an extent that any sign of an outer ITB disappears. The variation of the normalised heat flux caused by these ELMs is shown in Fig.8a, covering a period between the first and the second type-I ELMs ($6.49s<t<6.55s$) and in Fig.8b, covering a time interval after the second ELM ($6.58s<t<6.62s$). Each figure demonstrates a dependence of normalised heat flux $q_e/(n_e T_e^{5/2})$ on the parameter R/L_{T_e} at different radial locations. The dependence of the normalised heat flux $q_e/(n_e T_e^{5/2})$ on parameter R/L_{T_e} was approximated using formula (1). Dashed lines show the best fits of the approximations. They were used formally to deduce the critical $(R/L_{T_e})^{exp}_{cr}$ and stiffness factor C and their standard deviations. They are shown in Table 4 and 5 for time intervals $6.49s<t<6.55s$ and $6.58s<t<6.62s$, respectively. It is obvious that the rate of the flux variation changes significantly in the upper and lower parts of the curve for R=3.56m, which corresponds to the ITB location. The critical gradient model is not applicable inside ITB and approximation (1) produces large standard deviation for $(R/L_{T_e})^{exp}_{cr}$ and very small value for C as can be seen in Table 4. Fig.9 shows variation of stiffness parameters in the region between ITB and the plasma periphery.

Table 4. Stiffness factor and critical R/L_{T_e} deduced from experiment and predicted by theory. Standard deviations are shown in parenthesis. Pulse No's: 51573, $6.49s<t<6.55s$.

It should be noted that the stiffness parameters were not defined inside the region between the magnetic axis and R = 3.45m in the first shown time interval. The applied technique does not allow to deduce the regular part of the flux variation due to noise type fluctuations on the heat flux in this region (see curve at R = 3.45m in Fig.8a). Physically this means that the perturbation is strongly damped inside ITB (around R = 3.56m). After the second type-I ELM at t = 6.66s the ITB is strongly eroded and destroyed completely in the end. The perturbation penetrates deeper in the plasma and the heat flux variation becomes more regular as shown in Fig.8b for R = 3.4m and 3.45m, although the standard deviation remains large.

One can see that parameter R/L_{T_e} increases on average with transition from Fig.8a to Fig.8b for each given R, which is not inside the ITB. A solid curve on the right hand side of each graph shows the dependence in the region of the outer ITB at R=3.56m. Here the R/L_{T_e} decreases from 15 which is in the region typical of profile inside ITBs to 8 which is close to the magnitude which is typical of stiff standard H-mode profiles [18]. Such decrease in R/L_{T_e} value inside the ITB layer indicates the deterioration of ITB and its disappearance due to the perturbations caused by ELMs.

The character of the flux variation in the region between outer ITB and the plasma periphery to some extent is consistent with the Critical Gradient Model (CGM) although large standard deviations are found for $(R/L_{T_e})^{exp}_{cr}$ as can be seen from Table 4,5. The stiffness factor is close to what is observed in standard H-mode discharge or slightly above it. After the ITB destruction a manifestation of the stiffness can be seen deeper in the plasma at R = 3.4, 3.45m.

CONCLUSIONS.

Electron heat flux propagation has been analysed using the TRANSP code and ECE measurements of electron temperature in H-mode and optimised shear discharges in JET. The heat pulse associated with temperature perturbations caused by ELMs propagates in accordance with critical gradient model (CGM) [1,4,11-13] in a standard H-mode and hybrid scenario discharges in a region of $0.3<r/a<0.8$. The analysis allows the determination of the critical $(R/L_{T_e})^{exp}_{crit}$ and T_e profile stiffness factor C (eq.1). There is a difference between the theoretical predictions [7,13] of the critical $(R/L_{T_e})^{th}_{crit}$ and experimentally observed $(R/L_{T_e})^{exp}_{crit}$. It should be noted that the trends of radial variation of the theoretical predictions [7] and [13] are different, which may help to understand the nature of the difference between the two theories and experiment. The stiffness factor C in eq.(1) typically increases with a transition from the inner half to the outer half of the minor radius.

In ITB plasmas type-I ELMs cause a deterioration or destruction of the internal barriers. The critical gradient model and approximation (1) is inapplicable to the heat flux perturbations produced by large ELMs inside ITBs. Strong damping of the perturbation is observed inside ITB and it disappears in the region between magnetic axis and ITB. The heat flux evolve roughly in accordance with the critical gradient model in the region between ITB and plasma periphery. The stiffness factor C is close to what is observed in standard H-mode or slightly above it.

ACKNOWLEDGEMENT.

The author is grateful to Dr. P.Mantica and Prof. V.Parail for fruitful discussions, comments and recommendations. Special thanks to V.Drozdov for processing of the fast magnetic data used in equilibrium calculations and Abel inversion of interferometer data on the fast time scale by H.Leggate. This work was partly supported by the United Kingdom Engineering and Physical Sciences Research Council and by the European Communities under the contract of Association between EURATOM and UKAEA. The views and opinions expressed herein do not necessarily reflect those of the European Commission.

REFERENCES

[1]. Imbeaux F *et al 2001 Plasma Phys. Control. Fusion* **43** 1503
[2]. Ryter F *et al 2001 Phys. Rev. Lett.* **86** 2325
[3]. Hoang G T *et al* 2001 *Phys. Rev. Lett.* **87** 125001
[3]. Ryter F *et al 2003 Nucl. Fusion* **43** 1396
[4]. Garbet X *et al 2004 Plasma Phys. Control. Fusion* **46** 1351
[5]. Mantica P *et al 2004 Progress in Understanding Heat Transport at JET Fusion Energy 2004, 20th IAEA (Vilamoura, 2004)* (IAEA) EX/P6-18 http://www-pub.iaea.org/MTCD/Meetings/PDFplus/fusion-20-preprints/index.htm
[6]. Ryter F *et al 2005 Phys. Rev. Lett.* **95** 085001
[7]. Peeters A G *et al 2005 Phys. Plasmas* **12** 022505
[8]. Mantica P *et al 2002 Plasma Phys. Control. Fusion* **44** 2185
[9]. Garbet X *et al 2005 Plasma Phys Control Fusion* **47** 957
[10]. Sarazin Y *et al 2002 Plasma Phys Control Fusion* **44** 2445
[11]. Mantica P *et al 2006 Plasma Phys. Control. Fusion* **48** 385
[12]. Gentle K.W. *et al 2006 Plasmas Phys* **13** 012311
[13]. Weiland J *et al 2005 Plasma Phys. Control. Fusion* **47** 441
[14]. Goldstone R J *et al 1981 Comp Phys* **43** 61
[15]. Joffrin E *et al 2003 Nucl.Fusion* **43** 1167
[16]. Hawkes N C *et al 2002 Plasma Phys Control Fusion* **44** 1105
[17]. Baranov Yu F *et al 2005 Plasma Phys Control Fusion* **47** 975
[18]. Ryter F *et al 2006 Plasma Phys Control Fusion'Electron Transport Studies' EPS 2006 invited paper*
[19]. Tresset G *et al 2002 Nucl Fusion* **42** 520

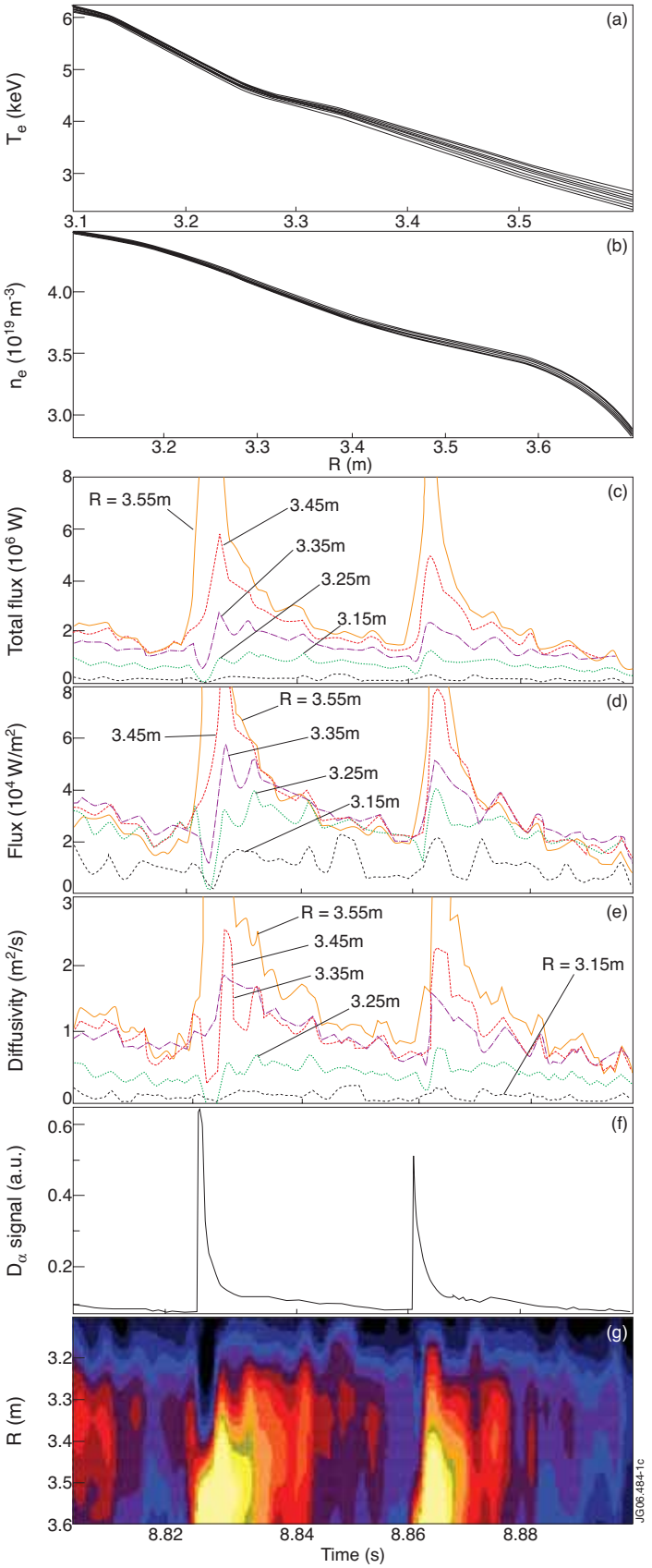

Figure1: (a) T_e profile variation between ELMs, b) density profile variation between ELMs c) total electron heat flux $\int q_e$ ds trough the plasma surface s, d) heat flux q_e, e) electron heat diffusivity χ_e, f) D_α signal, g) contour plot of q_e provides a qualitative picture of the perturbation of the heat flux in time and space. Bright colours represent higher amplitude of perturbation and dark colours lower amplitude. Magnetic axis and plasma boundary are at R_o=3.04m and R_b=3.84m, respectively. Pulse No: 62494, t=8.8-8.9s.

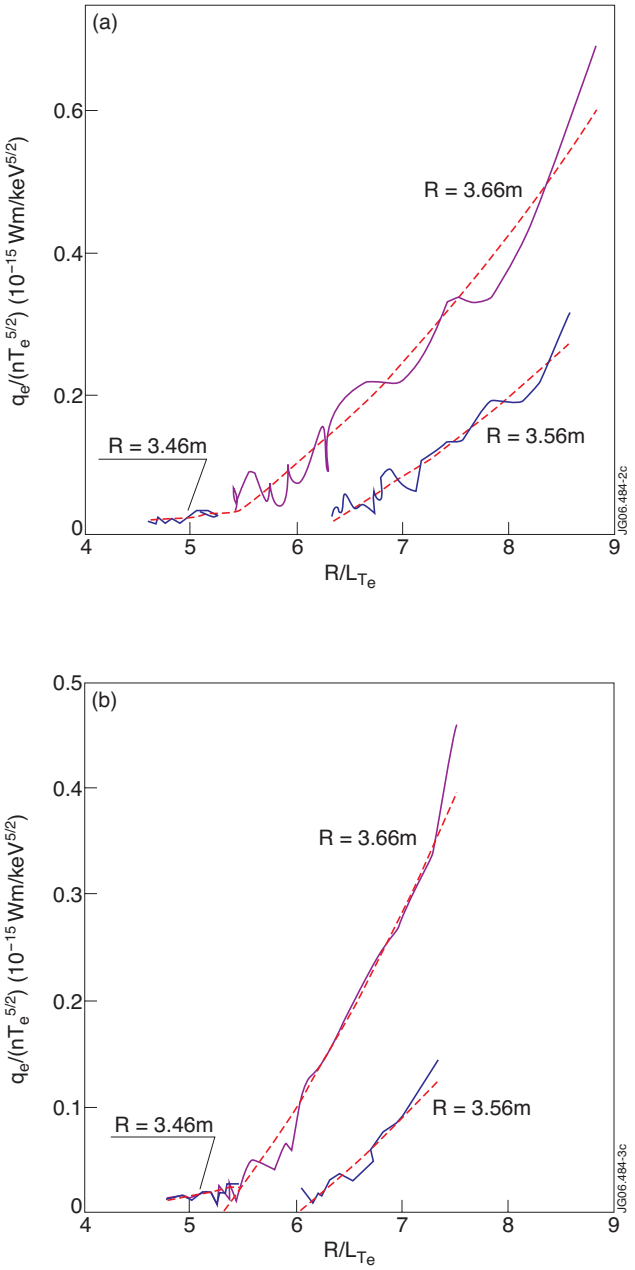

Figure 2: Variation of $q_e/(n_eT_e^{5/2})$ between successive ELMs versus R/L_{T_e}, a) t=8.827-8.860s, b) t=11.515-11.540s, Solid lines- / $(n_eT_e^{5/2})$ q_e^{exp} at different radii, dashed lines-the best fit using formula (1). Magnetic axis and plasma boundary are at R_o=3.04m and R_b=3.84m, respectively. Pulse No: 62494.

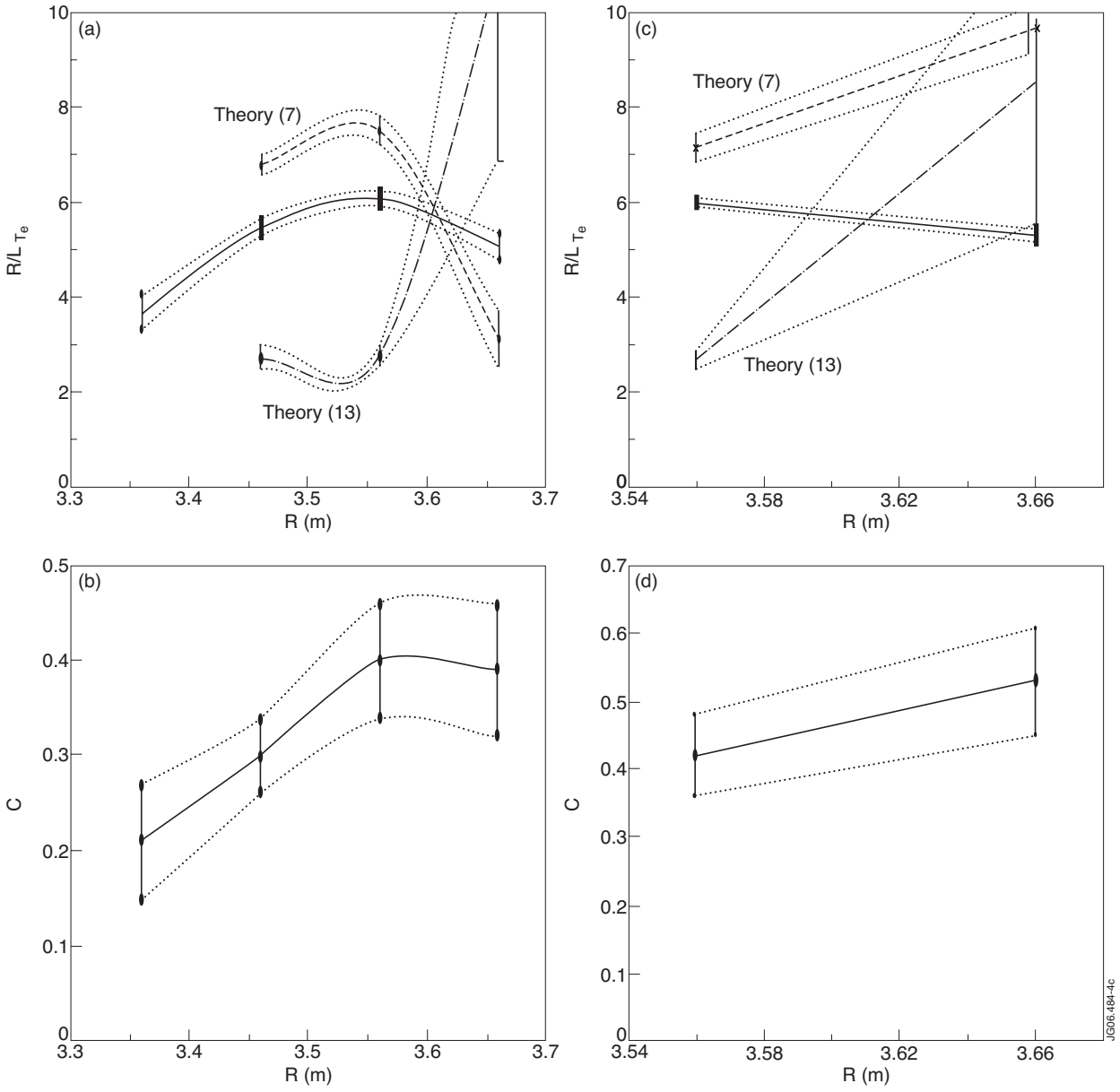

Figure 3: a,c) Solid line shows $(R/L_{T_e})^{exp}_{cr}$ corresponding to minimum χ^2 and its standard deviation is shown by vertical lines. Theoretical values of $(R/L_{T_e})^{th}_{cr1,2}$ [7,13] are shown by points on dashed lines. Theory is not applicable for R<3.4m as magnetic shear s<0.5. b,d) Stiffness coefficient C is shown by solid line and its standard deviation is shown by vertical lines. Expression (2) defines 'apparent' threshold, which is 10-20% larger than the real one [7]. This factor moves theoretical threshold [7] closer to the experimental values of $(R/L_{Te})_{cr}$ for R £3.55m. Anomalous increase in $(R/L_{T_e})^{th}_{cr2}$ for R>3.55m occurs due to a stabilising effect of the density gradient [13], which is probably not realistic for R/L_n>1. Pulse No: 62494, a,b) t=8.827-8.860s, c,d) t=11.515-11.540s.

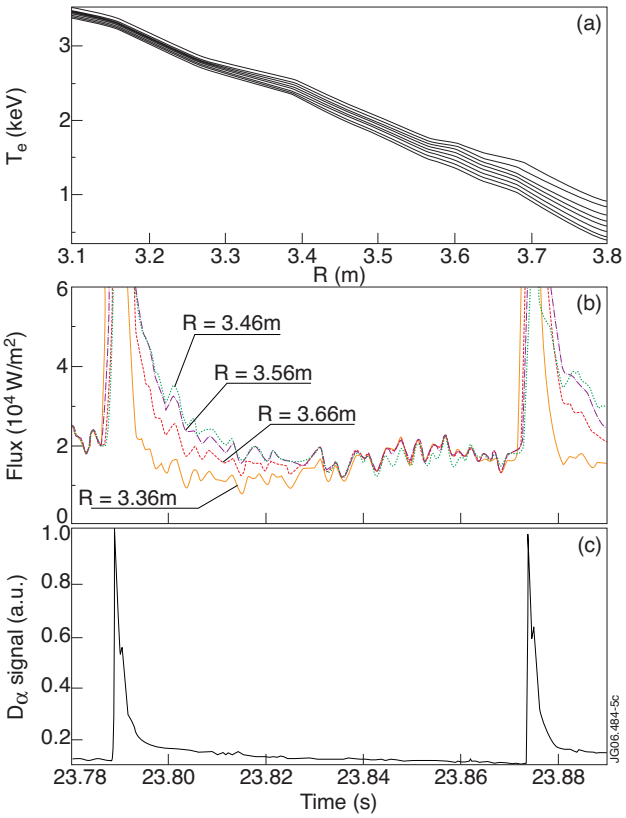

Figure 4: (a) T_e profile variation caused by ELMs, b) heat flux q_e, c) D_α signal. Magnetic axis and plasma boundary are at R_o=3.07m and R_b=3.87m, respectively. Pulse No: 61520, t=23.790-23.820s.

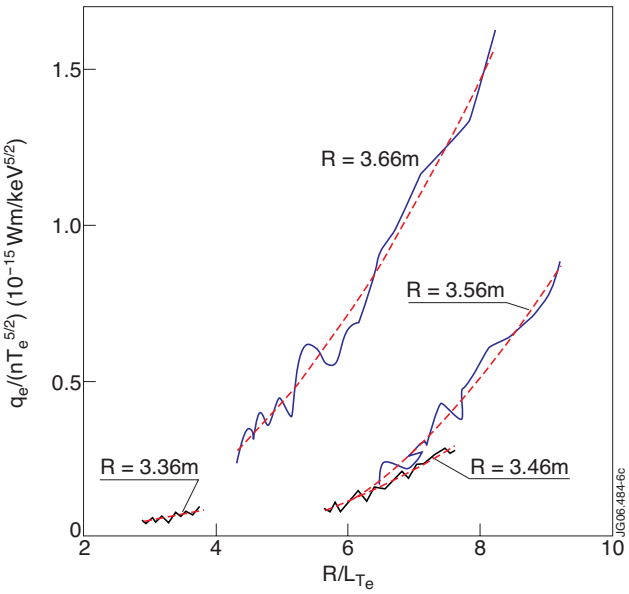

Figure5: Variation of $q_e/(n_eT_e^{5/2})$ between successive ELMs versus R/L_{T_e} at different radii. Solid lines- / $(n_eT_e^{5/2})$ q_e^{exp}, dashed or dotted lines - the best fit using formula (1). Magnetic axis and plasma boundary are at R_o=3.07m and R_b=3.87m, respectively. Pulse No: 61520, t=23.790-23.820s.

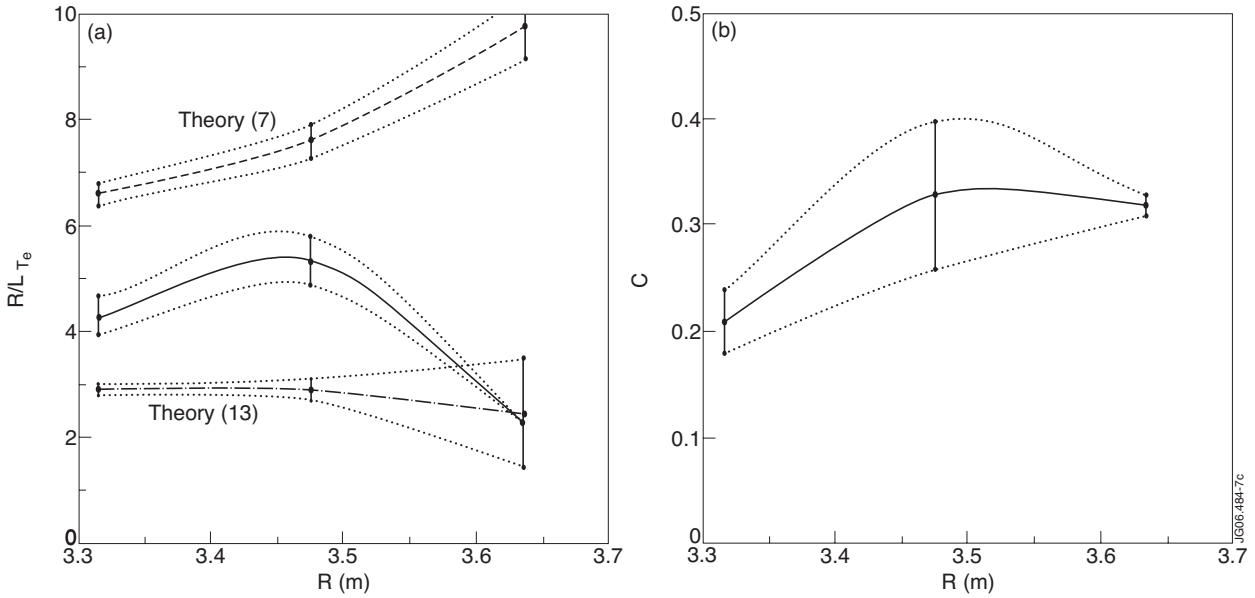

Figure 6: (a) Solid line shows $(R/L_{T_e})_{cr}^{exp}$ corresponding to minimum χ^2 and its standard deviation is shown by vertical lines. Theory [7,13] prediction are shown by points on dashed lines. Real $(R/L_{Te})_{cr}$ is 10-20% smaller than 'aparent' threshold of ref.[7] (see comments in Fig.3 captions). b) Stiffness coefficient C is shown by solid line and its standard deviation is shown by vertical lines. Pulse No: 61520, t=23.790-23.820s.

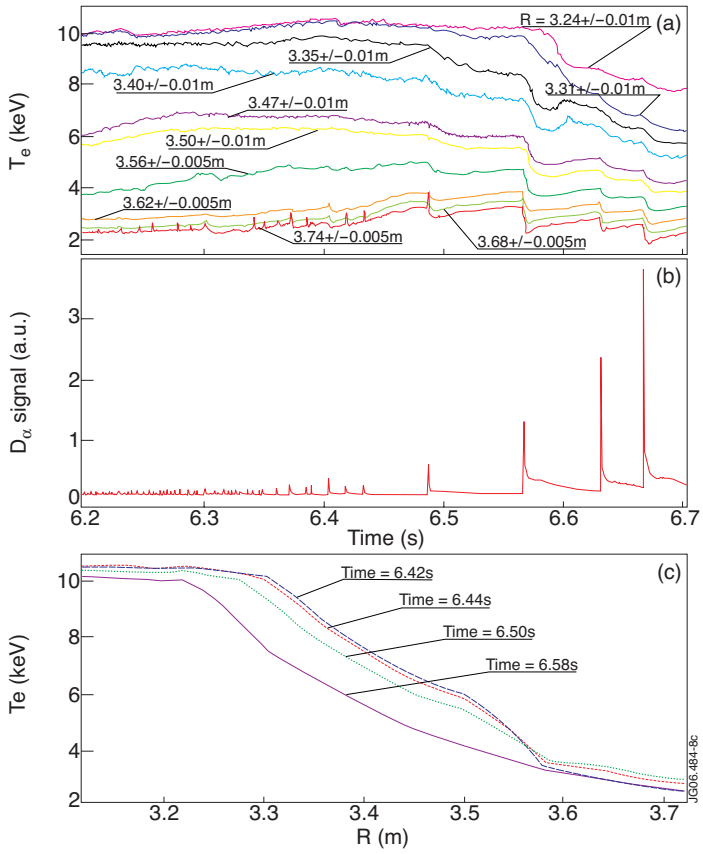

Figure 7: a) T_e variation vs. time at different radii, b) D_α-signal, c) T_e profiles. Outer ITB near R = 3.56m coexists with small benign type-III ELMs before t=6.487s and they cause only small temperature perturbations. Type-I ELMs after t = 6.487s cause large T_e perturbation penetrating deep into plasma (a). T_e gradient in the vicinity of ITB is reduced significantly after the first large ELM at 6.487s. ITB disappears completely after the second large ELM at t = 6.568s (b). The core ITB survives during all ELMs. It moves from the region around R = 3.36m at t = 6.2s to the region around R = 3.28m by t = 6.6s. Magnetic axis and plasma boundary are at R_o = 3.15-3.16m and R_b = 3.85m, respectively. Pulse No: 51573.

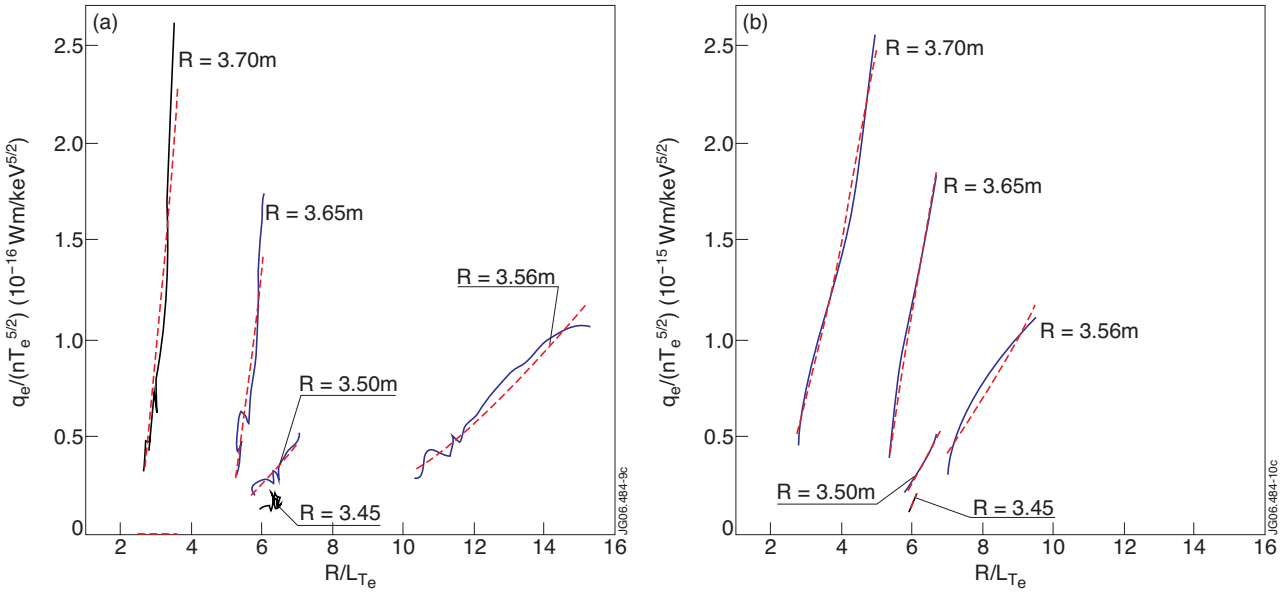

Figure 8: Variation of normalised heat flux versus R/L_{Te} at different radii between two type-I ELMs, a) 6.492s<t<6.55s, b) 6.580s<t<6.620s. Magnetic axis and plasma boundary are at R_o = 3.15-3.16m and R_b = 3.85m, respectively. Pulse No: 51573.

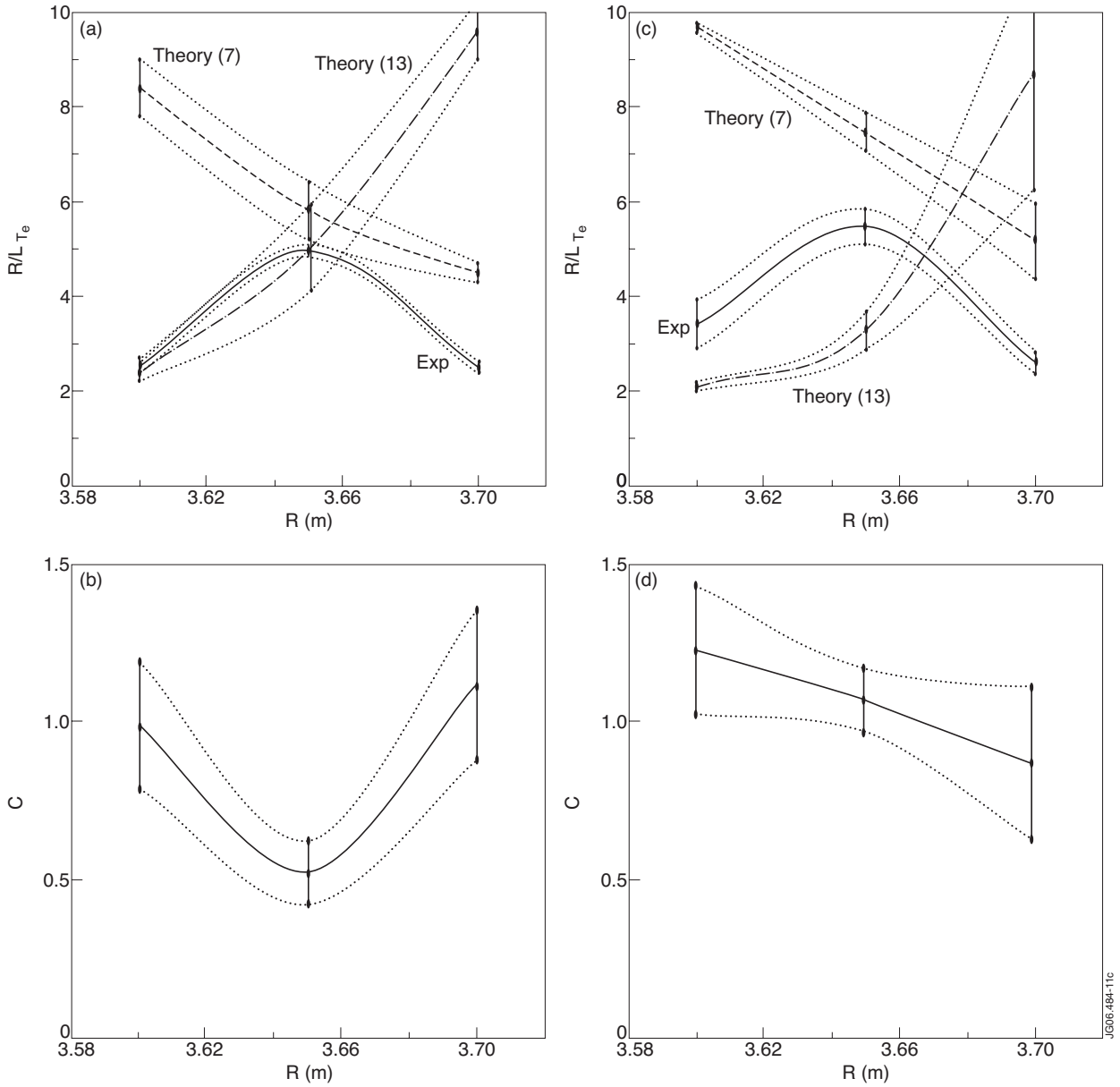

Figure 9. a,c) Solid line shows' $(R/L_{T_e})_{cr}^{exp}$ corresponding to minimum χ^2 and its standard deviation is shown by vertical lines. Theory [7,13] prediction are shown by points on dashed lines. Real $(R/L_{Te})_{cr}$ is 10-20% smaller than 'aparent' threshold of ref.[7] (see comments in Fig.3 captions). b,d) Stiffness coefficient C is shown by solid line and its standard deviation is shown by vertical lines. No data are shown for region inside ITB (R<3.58m) as the critical gradient model is not applicable inside ITB. a,b) 6.492s<t<6.55s, c,d) 6.580s<t<6.620s. Pulse No: 51573.